

Fluorescent Probes

International Edition: DOI: 10.1002/anie.201712614

German Edition: DOI: 10.1002/ange.201712614

Hybrid Indicators for Fast and Sensitive Voltage Imaging

Yongxian Xu⁺, Luxin Peng⁺, Sicong Wang⁺, Anqi Wang⁺, Ruirui Ma, Ying Zhou, Jiahe Yang, De-en Sun, Wei Lin, Xing Chen, and Peng Zou*

Abstract: Membrane voltage is an important biophysical signal that underlies intercellular electrical communications. A fluorescent voltage indicator is presented that enables the investigation of electrical signaling at high spatial resolution. The method is built upon the site-specific modification of microbial rhodopsin proteins with organic fluorophores, resulting in a hybrid indicator scaffold that is one of the most sensitive and fastest orange-colored voltage indicators developed to date. We applied this technique to optically map electrical connectivity in cultured cells, which revealed gap junction-mediated long-range coupling that spanned over hundreds of micrometers.

Membrane voltage controls many fundamental aspects of cellular physiology. The transmembrane electric field arises from the action of ion-selective channels and pumps, and it acts upon a range of membrane-embedded biomolecules, such as voltage-gated ion channels and receptors.^[1] As exemplified in neural and cardiac tissues, membrane voltage is often tightly regulated through intercellular communications such as chemical and electrical synapses.^[2,3] Understanding the function of these systems requires recording membrane voltage dynamics with high spatial and temporal resolutions. To this end, various voltage-sensitive fluorescent indicators have been developed, including both synthetic dyes^[4] and protein-based sensors.^[5] While protein-based sensors are readily targetable to specific cell types, their brightness and photostability are typically worse than syn-

thetic dyes. In the present study, we sought to create a hybrid voltage indicator that combines the merits of small molecules and proteins.

Our method capitalizes on the electrochromic Förster resonance energy transfer (eFRET) mechanism, initially discovered in microbial rhodopsins.^[6–8] As shown in Figure 1, membrane voltage fluctuations lead to changes in the absorption spectrum of rhodopsin, which could be probed with a site-specifically ligated organic fluorophore donor (Supporting Information). We called this design FlareFRET, for fluorophore ligation-assisted rhodopsin eFRET.

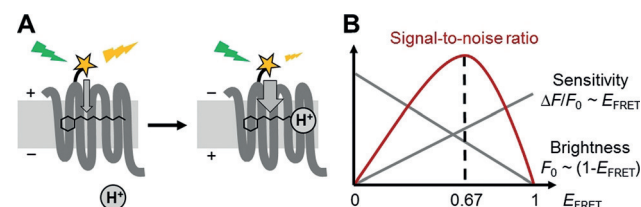


Figure 1. The FlareFRET design. A) A small molecule fluorophore (yellow star) is site-specifically ligated to rhodopsin (gray). Membrane voltage modulates the acid–base equilibrium of a Schiff base. When the cell undergoes depolarization, Schiff base protonation increases the absorption and leads to fluorescence quenching of the ligated fluorophore. B) Theoretical calculation shows that as baseline FRET efficiency (E_{FRET}) increases, voltage sensitivity increases linearly while the brightness decreases. In the regime of shot-noise limit, the signal-to-noise ratio is optimal when E_{FRET} is 67% (see discussion in the Supporting Information).

[*] Y. Xu,^[†] L. Peng,^[†] S. Wang,^[†] A. Wang,^[†] R. Ma, Y. Zhou, J. Yang, D. Sun, Dr. W. Lin, Prof. Dr. X. Chen, Prof. Dr. P. Zou
College of Chemistry and Molecular Engineering, Synthetic and Functional Biomolecules Center, Beijing National Laboratory for Molecular Sciences, Key Laboratory of Bioorganic Chemistry and Molecular Engineering of Ministry of Education, Peking University Beijing 100871 (China)
E-mail: zoupeng@pku.edu.cn

Y. Xu,^[†] A. Wang,^[†] Prof. Dr. X. Chen, Prof. Dr. P. Zou
Peking-Tsinghua Center for Life Sciences, Beijing 100871 (China)
Prof. Dr. P. Zou
PKU-IDG/McGovern Institute for Brain Research
Beijing 100871 (China)

J. Yang
MRC Human Immunology Unit
Weatherall Institute of Molecular Medicine, University of Oxford
Oxford, Oxfordshire OX3 9DS (UK)

Y. Xu,^[†]
School of Life Sciences, Tsinghua University, Beijing, 100084 (China)

[†] These authors contributed equally to this work.

Supporting information and the ORCID identification number(s) for the author(s) of this article can be found under:
<https://doi.org/10.1002/anie.201712614>.

We chose PRIME (probe-incorporation mediated by enzyme) labeling technique to construct FlareFRET sensors, because it offered a combination of small tag size, targeting specificity and fast reaction kinetics.^[9,10] Fluorophore ligation was achieved via two steps (Figure 2 A). In the first step, an engineered lipoic acid ligase mutant (^{W37V}LplA) recognized a 13-amino-acid acceptor peptide (LAP) that was fused to rhodopsin, and ligated a picolyl azide (pAz) moiety to its lysine side chain. Subsequently, an alkyne-derivatized fluorophore was conjugated to pAz via Cu^I-catalyzed azide–alkyne [3+2] cycloaddition (CuAAC) reaction.

We started by comparing several rhodopsin candidates for their tolerance of LAP insertions. In human embryonic kidney (HEK) cells, *Acetabularia acetabulum* rhodopsin (Ace)^[7] showed the best membrane trafficking (Supporting Information, Figure S1), which we used for subsequent studies. The proton-pumping activity of Ace was reduced with a single mutation D81N (Supporting Information, Figure S2).^[7] We inserted LAP at various locations in the Ace sequence and compared the PRIME labeling efficiency using Cy3 as the fluorescence reporter. As shown in Figure 2 B, Cy3

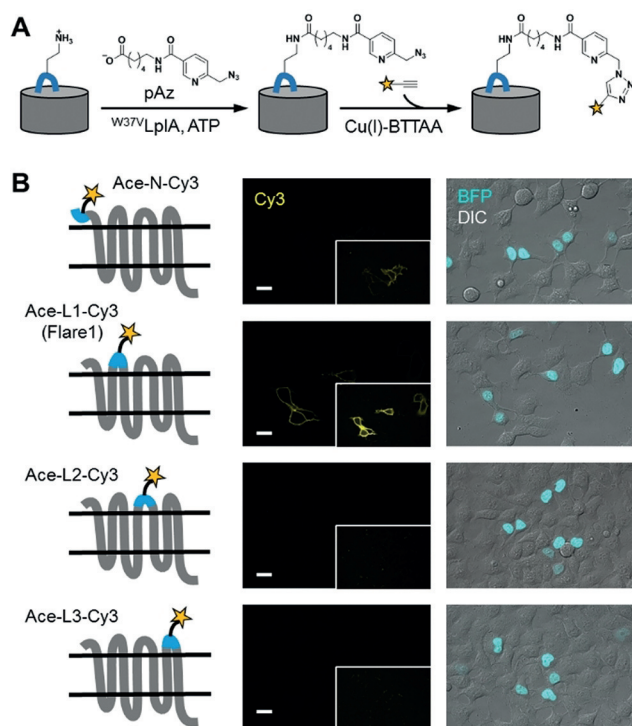


Figure 2. Site-specific protein labeling on a live cell surface via PRIME and click chemistry. A) An exogenously supplied PRIME ligase w^{37V} LpIa covalently attaches a picolyl azide (pAz) probe onto LAP-fused rhodopsin protein. Subsequently, pAz-modified rhodopsins are chemoselectively derivatized with a terminal alkyne-fluorophore conjugate by chelation-assisted CuAAC. B) Fluorescence images of living HEK cells labeled with FlareFRET sensors after two-step labeling. Left: FlareFRET designs. LAP tag is shown in blue. Yellow star represents Cy3. Middle: confocal images of Cy3, with fluorescence intensities normalized to the same level. Insets show images with enhanced contrast. Right: confocal images of histone-BFP (a transfection marker) overlaid on DIC images of the same fields of view. DIC: differential interference contrast. Scale bars: 20 μm .

signal was highest when LAP was inserted into the first extracellular loop of Ace (Ace-L1). Ace-L1 had approximately twice the labeling intensity of N-terminal LAP (Ace-N) fusion (Supporting Information, Figure S3), but was weaker than mNeonGreen fluorescence from Ace2N-2AA-mNeon (Supporting Information, Figure S4).^[7] Little labeling signal was observed when LAP was inserted to other extracellular loops, which we attributed to poor expression (Supporting Information, Figure S5). CellTiter-Glo assay showed that these labeling steps had negligible toxicity to HEK cells (Supporting Information, Figure S6). We thus focused on Ace-L1 and Ace-N for further engineering.

Taking advantage of the broad absorption spectrum of Ace,^[7] we created a palette of FlareFRET sensors by conjugating dyes with different colors, including Alexa Fluor 488 (AF488), Cy3, Alexa Fluor 594 (AF594), and Cy5 (Figure 3A; Supporting Information, Figure S7). Because these reagents were not membrane-permeable, labeling was restricted to the cell surface (Figure 3B; Supporting Information, Figure S7). In comparison, Ace2N-2AA-mNeon produced bright intracellular signal that was indicative of protein retention in the secretory pathway. Increasing the

membrane fraction of fluorescence signal is advantageous for voltage imaging.

To evaluate voltage sensitivity, we used whole-cell patch clamp technique to control the membrane voltage of labeled HEK cells, while simultaneously recording the fluorescence signal under the microscope. As we varied the membrane voltage across the physiologically relevant range between -100 mV and 50 mV, the fluorescence signal from these hybrid voltage indicators changed almost linearly (Figure 3C; Supporting Information, Figure S7 and Figure S8). The highest sensitivity was observed in Ace-L1 conjugated with Cy3 (Ace-L1-Cy3), achieving $-\Delta F/F$ of $35.9 \pm 0.8\%$ (per 100 mV, normalized to F at -70 mV; Supporting Information, Movie S1). This sensor, which we named as Flare1, had similar voltage sensitivity in HeLa ($36.0 \pm 1.4\%$) and Chinese Hamster Ovary (CHO) cells ($30.9 \pm 1.9\%$; Supporting Information, Figure S9 and Table S2). In comparison, Ace2N-2AA-mNeon showed only $9.4 \pm 0.6\%$ fluorescence change under the same condition (Figure 3C; Supporting Information, Movie S1). Both Ace-L1-AF488 ($28.2 \pm 0.9\%$) and Ace-L1-AF594 ($23.9 \pm 1.3\%$) had lower sensitivity than Flare1, whereas Ace-L1-Cy5 had negligible response ($5.4 \pm 0.6\%$). We noted that the maximum emission wavelength of Cy3 coincided with the absorption maximum of Ace.^[7] This spectral dependence of voltage sensitivity was expected from the eFRET mechanism.

Voltage sensitivity also depends on the protein scaffold. Ace-N sensors overall are less sensitive than Ace-L1 sensors (Supporting Information, Figure S7 and Table S2). We also explored other site-specific protein labeling techniques, including HaloTag,^[11] SNAP-tag,^[12] and streptavidin labeling (Supporting Information, Figure S10).^[13] These sensors all exhibited lower voltage sensitivity than Flare1 (Supporting Information, Table S2), which we attributed to long donor-acceptor distances owing to the bulky tag size (HaloTag is 34 kDa, SNAP-tag 19 kDa, streptavidin 53 kDa, whereas LAP tag is only 1.6 kDa). We noticed slight hysteresis in the F - V response curves of FlareFRET sensors, which likely arises from voltage-induced conformational changes in Ace. Taken together, the above screening efforts identified Flare1 as the most sensitive hybrid voltage indicator.

To quantify the response kinetics, we stepped the membrane voltage between -70 mV and 30 mV, which induced bi-exponential fluorescence responses in FlareFRET sensors (Figure 3D; Supporting Information, Figure S7). As shown in the Supporting Information, Figure S11 and Table S2, both Ace-L1 and Ace-N sensors responded within milliseconds. Flare1 had a dominating fast component with time constant $\tau = 0.92 \pm 0.03$ ms ($96.0 \pm 0.7\%$) during depolarization and $\tau = 1.41 \pm 0.04$ ms ($91.0 \pm 0.7\%$) during hyperpolarization. Consistent with a previous report,^[7] Ace2N-2AA-mNeon exhibited complex response kinetics, in which a rapid initial overshoot was followed by a slower decay to steady-state fluorescence on a time scale of about 100 ms. The fast and simple response kinetics of Flare1 could simplify data analysis when extracting voltage information from optical traces.

Our theoretical model of eFRET voltage sensing predicts a positive correlation between voltage sensitivity and baseline FRET efficiency, E_{FRET} (see the Supporting Information). To

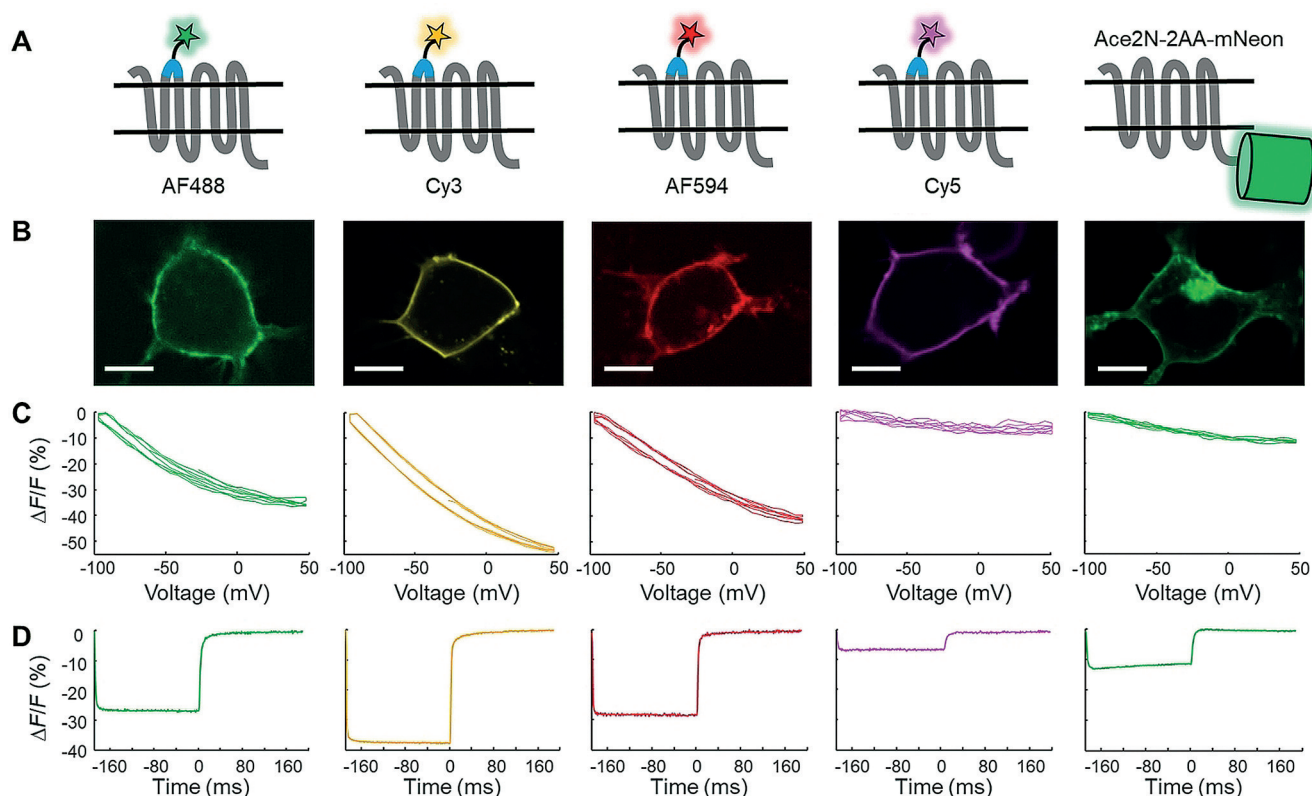


Figure 3. Voltage response of FlareFRET sensors and Ace2N-2AA-mNeon. A,B) Representations and corresponding confocal images of fluorescently labeled HEK cells. Scale bars: 10 μm . C) Fluorescence as a function of membrane voltage. Each trace is a single trial of 4 ramp cycles. See the Supporting Information, Figure S8 for image series used to construct the F - V response curves. D) Fluorescence response to a stepping membrane voltage between -70 mV and 30 mV.

verify this model, we calculated FRET efficiencies based on fluorescence lifetime measurements in HEK cells, which have resting membrane voltage of about -40 mV.^[14] The excited-state decay of Flare1 can be fitted with a bi-exponential function, with a fast component lifetime of 0.177 ± 0.006 ns (81.1%) and a slow component of 0.968 ± 0.041 ns (18.9%; Supporting Information, Figure S12 and Table S3). In the absence of FRET, the lifetime of cell surface-targeted Cy3 is almost two-fold longer (fast: 0.359 ± 0.003 ns, 65.2%; slow: 1.519 ± 0.017 ns, 34.8%). From these data, we calculated E_{FRET} of Flare1 to be 56.8% (see the Supporting Information). For comparison, both Ace-N-Cy3 (40.5%) and Ace2N-2AA-mNeon (25.1%) had lower E_{FRET} than Flare1. Our model also suggests that the signal-to-noise ratio (SNR) is optimal when E_{FRET} reaches 67%. Notably, this level of energy transfer efficiency has never been achieved by fluorescent protein-based eFRET sensors,^[6] which is presumably due to the bulky size of their β -barrel scaffold. On the other hand, Flare1 has FRET efficiency that approaches this optimal range. Taken together, these data agreed with our theoretical model and highlighted the advantage of small tag size in FlareFRET hybrid voltage indicators.

We applied Flare1 to investigate the electrical connectivity in a cell population. Gap junction channels are specialized ion-conducting intercellular connections that enable direct electrical coupling between neighboring cells. These channels are known to contribute to cardiac activity, neuronal signal-

ing, and pancreatic secretion.^[2,3,15] We used HEK cells as a model to demonstrate the power of voltage imaging with Flare1 (Figure 4A–C). After fluorescence labeling, we used whole-cell patch clamp to control the membrane voltage of a single cell. As we ramped the voltage between -100 mV and 50 mV, we observed fluorescence changes in neighboring cells as well as cells that were hundreds of micrometers away (Figure 4A–C). Voltage response decays as a function of distance, with a length constant of 114 μm (Supporting Information, Figure S13), which, according to our modeling in the Supporting Information, is consistent with estimates of the electrophysiological properties of gap junction channels. In negative control experiments, no electrical connectivity was observed in the presence of gap junction blocker 2-aminoethoxydiphenyl borate (2-APB), or in HeLa cells that lack connexins to form gap junction channels (Figure 4A–C). This experiment demonstrated the power of Flare1 voltage imaging in revealing intercellular electrical communication.

Given the sensitivity and speed of Flare1, it should be able to detect neuronal action potentials. Indeed, in voltage-clamped HEK cells, Flare1 was able to track simulated action potential spike trains (see the Supporting Information) with $-\Delta F/F$ of about 28% and the spike detection SNR ranging between 21 and 53 (Figure 4D–H). In cultured rat hippocampal neurons, both Ace-N and Ace-L1 traffic to the plasma membrane and can be labeled with alkyne–fluorophore conjugates via CuAAC (Supporting Information, Figure S14).

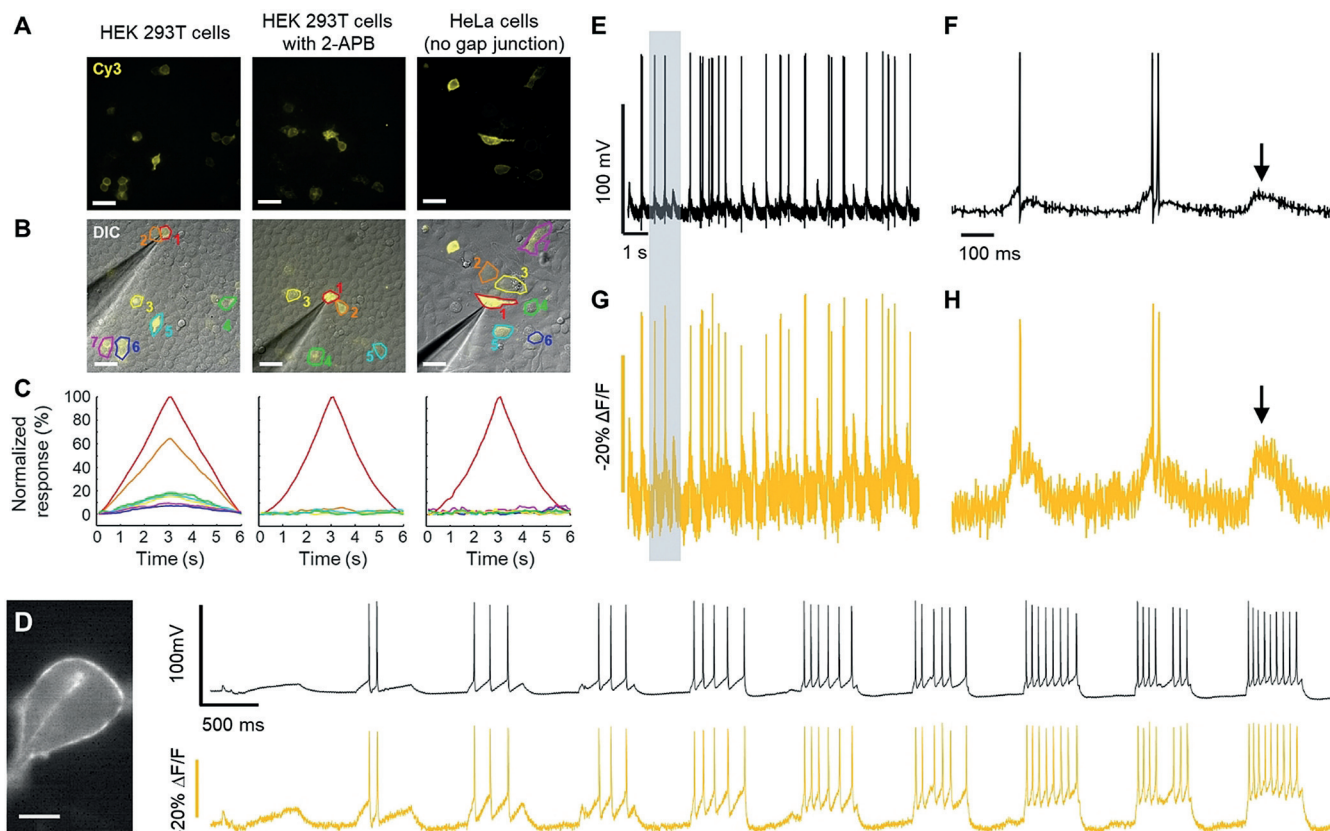


Figure 4. Optical mapping of electrical connectivity and simulated action potential waveforms with Flare1. A)–C) Optical mapping of electrical connectivity in HEK cells and HeLa cells with Flare1. Left: HEK cells labeled with Flare1; Middle: Flare1-labeled HEK cells in the presence of gap junction blocker 2-aminoethoxydiphenyl borate (2-APB). Right: HeLa cells labeled with Flare1. A) Representative fluorescence images of cells expressing Flare1. B) Differential interference contrast (DIC) images of the same fields of view. Regions of interest (ROIs) are marked in colored polygons. C) Normalized fluorescence responses to command voltage (a single trial of four -100 mV to 50 mV cycle) for each group. Colored traces correspond to ROIs with the same color code in (B). D) A simulated action potential spike trains (top, black trace) was applied to a Flare1-labeled HEK cell via voltage clamp. Flare1 fluorescence response was simultaneously recorded (bottom, yellow trace). E) Simulated spontaneous action potential waveforms applied to the HEK cell. F) Magnification of the voltage fluctuations under the shaded region shown in (E). G), H) Flare1 fluorescence response to the voltage waveforms in (E) and (F), respectively. Black arrows indicate a subthreshold voltage fluctuation. Scale bars: $50\ \mu\text{m}$ in (A) and (B), $10\ \mu\text{m}$ in (D).

However, we observed greatly reduced neuronal excitability and action potential firing rates (Supporting Information, Figure S15), which is mainly due to the addition of copper. Although these labeling reagents have negligible toxicity in HEK cells (Supporting Information, Figure S6), they appear to be too harsh for neurons. This calls for the development of milder probe conjugation methods.

In summary, we have created a palette of hybrid voltage indicators (Figure 5). Among these, Flare1 represents one of the most sensitive ($-\Delta F/F = 35.9\%$ per 100 mV) and fastest (sub-millisecond response) orange-colored fluorescent voltage indicators developed to date. The superior sensitivity of Flare1 has enabled optical mapping of electrical connectivity among cultured cells, which revealed gap-junction-mediated long-range coupling that spanned over hundreds of micrometers. Moreover, the kinetics and dynamic range of Flare1 are sufficient to report simulated action potential train waveforms. We envision that FlareFRET sensors will greatly expand the toolbox of voltage imaging, and the next goal is to apply these tools to visualize action potentials in neurons.

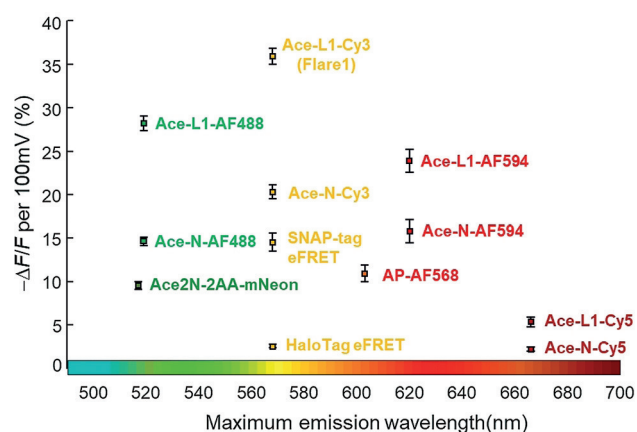


Figure 5. Summary of the voltage indicators reported herein. The horizontal axis represents the maximum emission wavelength, and the vertical axis represents voltage sensitivity in $-\Delta F/F$, normalized to the fluorescence at $V_m = -70$ mV. The text color represents the approximate fluorescence emission color based on the spectrum. Error bars represent s.e.m.

Acknowledgements

This work was supported by the National Natural Science Foundation of China (Grant 21673009, 21727806) and the Peking-Tsinghua Center for Life Sciences. P.Z. was supported by the National Thousand Young Talents Award.

Conflict of interest

The authors declare no conflict of interest.

Keywords: click chemistry · fluorescent probes · FRET · protein engineering · voltage imaging

How to cite: *Angew. Chem. Int. Ed.* **2018**, *57*, 3949–3953
Angew. Chem. **2018**, *130*, 4013–4017

-
- [1] A. E. Cohen, V. Venkatachalam, *Annu. Rev. Biophys.* **2014**, *43*, 211–232.
- [2] M. V. Bennett, R. S. Zukin, *Neuron* **2004**, *41*, 495–511.
- [3] S. Dhein, *Trends Pharmacol. Sci.* **1998**, *19*, 229–241.
- [4] E. W. Miller, *Curr. Opin. Chem. Biol.* **2016**, *33*, 74–80.
- [5] Y. Xu, P. Zou, A. E. Cohen, *Curr. Opin. Chem. Biol.* **2017**, *39*, 1–10.
- [6] P. Zou, Y. Zhao, A. D. Douglass, D. R. Hochbaum, D. Brinks, C. A. Werley, D. J. Harrison, R. E. Campbell, A. E. Cohen, *Nat. Commun.* **2014**, *5*, 4625.
- [7] Y. Gong, C. Huang, J. Z. Li, B. F. Grewe, Y. Zhang, S. Eismann, M. J. Schnitzer, *Science* **2015**, *350*, 1361–1366.
- [8] Y. Gong, M. J. Wagner, J. Zhong Li, M. J. Schnitzer, *Nat. Commun.* **2014**, *5*, 3674.
- [9] C. Uttamapinant, A. Tangpeerachaikul, S. Grecian, S. Clarke, U. Singh, P. Slade, K. R. Gee, A. Y. Ting, *Angew. Chem. Int. Ed.* **2012**, *51*, 5852–5856; *Angew. Chem.* **2012**, *124*, 5954–5958.
- [10] C. Uttamapinant, M. I. Sanchez, D. S. Liu, J. Z. Yao, A. Y. Ting, *Nat. Protoc.* **2013**, *8*, 1620–1634.
- [11] G. V. Los, L. P. Encell, M. G. McDougall, D. D. Hartzell, N. Karassina, C. Zimprich, M. G. Wood, R. Learish, R. F. Ohana, M. Urh, D. Simpson, J. Mendez, K. Zimmerman, P. Otto, G. Vidugiris, J. Zhu, A. Darzins, D. H. Klaubert, R. F. Bulleit, K. V. Wood, *ACS Chem. Biol.* **2008**, *3*, 373–382.
- [12] A. Keppler, S. Gendreizig, T. Gronemeyer, H. Pick, H. Vogel, K. Johnsson, *Nat. Biotechnol.* **2003**, *21*, 86–89.
- [13] P. Zou, A. Y. Ting, *ACS Chem. Biol.* **2011**, *6*, 308–313.
- [14] P. Thomas, T. G. Smart, *J. Pharmacol. Toxicol. Methods* **2005**, *51*, 187–200.
- [15] A. Sherman, J. Rinzel, *Biophys. J.* **1991**, *59*, 547–559.

Manuscript received: December 8, 2017

Revised manuscript received: January 23, 2018

Accepted manuscript online: February 13, 2018

Version of record online: March 8, 2018